Contents lists available at ScienceDirect

# Composites Science and Technology

# Effects of barrelling during axial compressive tests of cubic samples with isotropic, transversely isotropic and orthotropic elastic properties

Alexey Vorobyev[*], Ingela Bjurhager, Nico P. van Dijk, E. Kristofer Gamstedt

*Division of Applied Mechanics, Uppsala University, Box 534, SE-751 21, Uppsala, Sweden*

## ABSTRACT

For scarce materials, such as archaeological wood, cubic samples are often used instead of standardized prisms for mechanical tests, since the elasticity can be determined in all three directions within a single sample, but with such samples barrelling makes it difficult to identify the elastic properties. The purpose of the present study is firstly to numerically investigate the effects of barrelling in cubic samples during compressive testing; secondly to numerically investigate and compare barrelling on isotropic and transversely isotropic material parameters; thirdly to compare four strain measurement techniques using digital image correlation, strain gauges and direct readings from the testing machine and finally to estimate the error due to barrelling by implementing the experimentally obtained orthotropic material parameters to the numerical model. The presented relative errors provide information when the perturbation caused by barrelling is negligible or significant for various materials and strain measurements. As an example, the results of compressive tests on waterlogged archaeological oak impregnated with polyethylene glycol are discussed.

© 2016 Elsevier Ltd. All rights reserved.

## 1. Introduction

The determination of stiffness properties of orthotropic materials can be challenging. In the careful design of wood structures, the full orthotropic set of elastic parameters is needed [1], e.g. for the finite-element modelling of wood joints that are locally subjected to a triaxial stress state. Compressive experiments are generally considered to be a reliable method of determining engineering constants such as compressive strength, Young's moduli and Poisson's ratios. The general approach is to measure the material response due to an applied force. The procedure is straightforward and easy to perform due to the simplicity of the experimental installation and low demands on sample geometry. The ASTM D-143 standard [2,3] requires the usage of elongated rectangular prisms for the compressive testing together with strain gauges. For rare materials such as archaeological wood as exemplified in Fig. 1(a), it is more convenient to use cubic samples [4,5] to save material, since the same sample can be tested several times in different directions (typically radial, tangential, longitudinal) if the loads are applied within the elastic range and do not cause irreversible damage to the material. A disadvantage of compressive testing a cube rather the tensile testing of a dog-bone sample is that it can be difficult to ensure a homogeneous stress state due to geometrical imperfections in the sample [6]. Moreover, barrelling (as illustrated in Fig. 1(b, c)) during compressive loading [7], caused by friction between the platens and the sample makes it difficult to assess the non-uniform deformation in order to determine the elastic parameters, and the Poisson's ratios cannot be obtained directly under such constraints. The most common way to measure strain is by using either the loading platen position or electrical-resistance strain gauges. Nowadays, full field strain measurement techniques such as 3D/stereo-digital image correlation (DIC) [8], virtual fields method [9] and digital volume correlation [10] are increasingly being used. The strain-field measurement technique using DIC has been shown to possess advantages in comparison with the traditional strain gauges [11–13]. In particular, full-field measurements can help to improve the estimation of the stiffness parameters [8,14,15]. Despite technical difficulties in obtaining accurate elastic properties from the compressive testing of wooden cubes, it is still a reasonable choice of test method if the amount of available material is limited, as is the case for e.g. archaeological
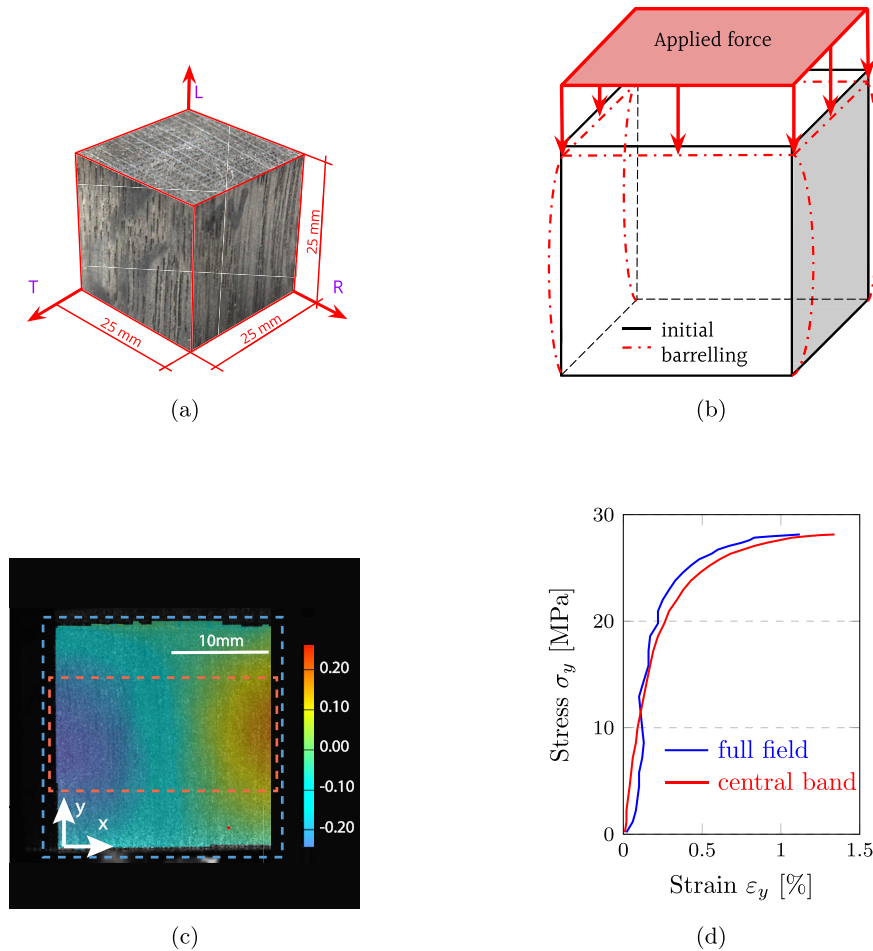
**Fig. 1.** (a) Vasa oak sample (b) Barrelling of an initially cubic shape. (c) DIC image of barrelling in Vasa oak sample during compressive testing including the displacement field. (d) Experimental stress-strain curves for Vasa oak sample.

material.

The presented work was initiated in order to better estimate the stiffness properties of water-logged and preservation-treated oak of the Vasa ship displayed at a public museum in Stockholm. The stiffness of the material is needed as input parameters in a finite-element model for use in the design of a future improved support system for the ship. The Vasa capsized in 1628, and was salvaged in 1961. The waterlogged ship was then immediately impregnated with polyethylene glycol (PEG) in an extensive conservation process aiming to prevent deformation during drying. Extensive research during the last decades has shown that the ship is nevertheless suffering from aggressive chemical degradation. Both the degradation [16] and the PEG impregnation [4] have had a negative effect on the mechanical properties of the ship, which is in need of a better support.

Mechanical experiments on cubic samples were conducted and numerically simulated by Odgaard and Linde [13]. They conducted two independent strain measurements using the optical and extensometer techniques during the non-destructive uniaxial compression of cancellous bone. Numerical simulation of the experiment assumed isotropy and homogeneity. They concluded that Young's modulus of was underestimated by about 20% using the extensometer technique. Compressive testing of on prismatic samples with orthotropic properties were previously simulated by Toftegaard [6] who investigated the effect of geometrical imperfections on the engineering elastic constants. In his work, Toftegaard compared the simulated strain field to the measurements of strain gauges, and obtained good agreement between the simulated and experimental data.

In mathematical simulations Chen [17] compared the deformation behaviour of samples with geometrical imperfections supported by a locked hemispherical seat with those of conventional platens. This is useful for rigid platens which cannot adjust to sample geometry to spread the loads more evenly over the contact area.

The purpose of the present work is to investigate how the occurrence of barrelling affect the accuracy of the elastic properties obtained from three different types of material behaviour, namely isotropic, transversely isotropic and orthotropic elastic properties, in ranges applicable to archaeological wood. The intention of the numerical study in the present work has been to estimate how large the measurement errors can be due to the inevitable barrelling formation, and which strain measures are the most suitable to reduce such errors.

In addition, four strain measurement techniques using DIC (full field and central band), strain gauges (recommended by the standard [2,3]) and direct compressive platen displacement are simulated and compared with respect to assess the magnitude of the resulting errors. The results can help to estimate the errors induced by the different strain measurement methods.

## 2. Materials and methods

### 2.1. Numerical model

The finite element program COMSOL Multiphysics 4.4 [18] was used for the numerical simulations. A cube with unit dimensions was modelled with 3D solid elements. The compliance of the rig was neglected since the platens were assumed to be rigid, leading to uniform normal displacement on the loaded surfaces. The compressive loading was simulated as a downward vertical displacement, the magnitude of which was set to 1% of the specimen height, or as 0.25 mm for a cube of 25 mm height. A mesh refinement study showed that a $10 \times 10 \times 10$ mesh of 1000 quadratic brick elements would provide sufficiently accurate results for the purpose of this study. Each quadratic brick element corresponds to the dimensions of $2.5 \times 2.5 \times 2.5$ mm$^3$ in the experiment.

The main cause of barrelling is the restraining friction between platens and specimen [13,19,20].

To simulate the effect of friction, we have introduced line springs with spring constant $K$ (N/m$^2$) that represent the friction in the model. These springs are evenly distributed along the edges on the top and the bottom of the cube as shown in Fig. 2. For $K = 0$ (N/m$^2$) the displacement of the edges is unconstrained, and for $K > 0$ (N/m$^2$) the edges are partially constrained up to the extreme case where the edges are completely constrained when $K = \infty$ (N/m$^2$). It should be noted that $K$ is not a physical friction constant, such as the Coulomb friction over the contact area, but serves well to simulate numerically the effect of contact friction. To assess the effects of barrelling on the stiffness measurement, an easily measurable parameter is required, unlike the line spring constant or a coefficient of static friction, $\mu$. An effect of friction closely related to barrel formation as the degree of slippage at the contact face, and we define this slippage as $\delta/\delta_{max}$, where $\delta$ is the lateral displacement and $\delta_{max}$ is the maximum displacement occurring when the static friction is zero. Thus, $\delta/\delta_{max} = 0$ corresponds to no slippage with $K = \infty$, and $\delta/\delta_{max} = 1$ corresponds to full slippage with $K = 0$ and $\mu = 0$. The slippage $\delta$ is directly measurable from the change in edge positions of the cube when deformed, and $\delta_{max}$ can be calculated from the deformed cube with no barrelling. It is also possible to simulate the contact between the platens and the sample. However, it will restrict the results to the specific amount of friction for a particular sample. In practice, the friction varies between the samples and materials.

### 2.2. Material input parameters

Isotropic, transversely isotropic and orthotropic linear elastic
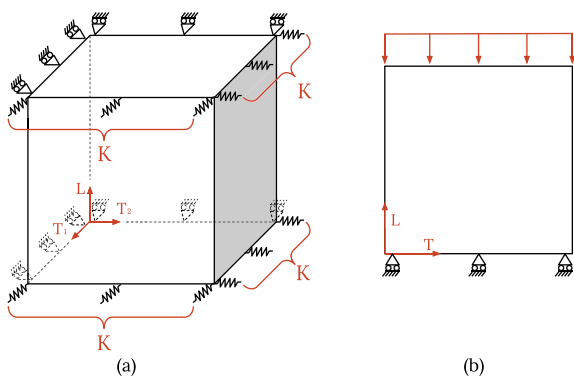


Fig. 2. Model of cubic sample used in the FEM simulation. (a) Horizontal boundary conditions and (b) vertical boundary conditions.

behaviour was investigated. Wood and composite materials are known to be anisotropic, although they are occasionally assumed to be transversely isotropic if two material axes have similar elastic properties. The simplified isotropic case is added as reference. The relationships between the elastic properties are listed in Table 1. Two parameters $a$ and $b$ were introduced to give a continuous transition between complete isotropy and transverse isotropy, while maintaining the symmetry conditions of the stiffness tensor. The first parameter, $a$, controls the relationship between the stiffnesses in the longitudinal and transverse directions as well as the corresponding Poisson's ratio. The second parameter, $b$, controls the out-of-plane shear modulus. The remaining three Poisson's ratios were obtained from the symmetry principle relations for the stiffness tensors [21]. The parameters $a$ and $b$ were fitted to the experimental elastic values of wood and some composite materials are shown in Table 2. For these orthotropic wood and composite materials, $a = 10$ and $b = 2$ were found to provide a suitable compromise for a common transversely isotropic material. In the isotropic case, $a = 1$ corresponds to a uniform Young's moduli $E$ and Poisson's ratio $\nu$ in all directions. The orthotropic material was simulated using experimental input parameters obtained from the experiments using DIC [5].

### 2.3. Strain measuring methods

Four realistic ways of measuring strain were considered in the simulations. These strains are a result of the imposed displacement of opposite faces of the unit cube by 0.01, corresponding to an average strain of 1%. The strains given by the simulation are:

- The average strain in the $x$ and $y$ directions over the entire analysed cube face (Full field), as shown with blue dashed line in Fig. 1(c).
- The average strains in the $x$ and $y$ directions over a centered region spanning the width and covering 60% of the total analysed cube face, as shown with red dashed line in Fig. 1(c). This region of interest was chosen to represent DIC measurements away from the constrained regions affected by restrained slippage along the platens (Central band).
- The average strain between two points in the $x$ and $y$ directions, respectively, located close to the centre of the cube face. This corresponds to the zone in which the strains are determined by the strain gauge as suggested in the ASTM D143 standard (Strain gauges) [22].
- The average strain based directly on the measurements in the universal testing machine from the displacements of the compression platens (Basic method)

### 2.4. Experimental procedures

An Instron universal testing machine with 100 kN load cell was used to carry out static tests. Special care was taken to prepare almost exactly cubic samples in size $25 \times 25 \times 25$ mm$^3$ in size. The opposite faces of each cube were machined with a parallelism tolerance of 0.01 mm. Initial tests were conducted on dummy wood specimens in order to find the approximate elastic loading range for all specimen orientations. Full-field displacements were observed with a DIC equipment GOM Aramis stereo system 5M. The distance to the measured object was 300 mm. The DIC settings were 19 pixel sized quadrangle faces and steps of 15 pixels, which after calibration resulted in an average intersection deviation of 0.0602 pixels. The surfaces of the specimens were spray-painted with speckles for better contrast. The applied force values were continuously recorded by the DIC system during testing, and stored together with the

**Table 1**
Engineering elastic constants used in the model.

| $E_{T1} = E_{T2}$ (GPa) | $E_L$ (GPa) | $G_{LT1} = G_{LT2}$ (GPa) | $G_{T1T2}$ (GPa) | $\nu_{T1L} = \nu_{T2L}$ | $\nu_{T1T2}$ |
|---|---|---|---|---|---|
| $E$ | $aE$ | $\frac{(b[a-1]+1)E}{2(1+\nu)}$ | $\frac{aE}{2(1+\nu)}$ | $\frac{\nu}{a}$ | $\nu$ |

Note: $E = 1$; $\nu = 0.25$; Parameter $a = 1$ for the isotropic and $a = 10$ for the transversely isotropic material model; Shear stiffness parameter $b = 1$ for isotropic and $b = 2$ for transversely isotropic.

**Table 2**
Typical engineering properties of orthotropic and transversely isotropic materials.

|  | Vasa oak (ref. nr. 65742) [5] | Graphite-polymer composite [21] | Glass-polymer composite [21] | S2 glass reinforced epoxy [21] |
|---|---|---|---|---|
| $E_{T1}$ (GPa) | 0.60 | 12.10 | 15.20 | 14.7 |
| $E_{T2}$ (GPa) | 0.35 | 12.10 | 15.20 | 14.7 |
| $E_L$ (GPa) | 6.75 | 155.0 | 50.00 | 49.3 |
| $G_{LT2}$ (GPa) | 0.62 | 4.40 | 4.70 | 6.8 |
| $G_{T1T2}$ (GPa) | 0.14 | 3.20 | 3.28 | 4.9 |
| $G_{LT1}$ (GPa) | 0.33 | 4.40 | 4.70 | 6.8 |
| $\nu_{LT1}$ (−) | 0.37 | 0.248 | 0.254 | 0.296 |
| $\nu_{T1T2}$ (−) | 0.30 | 0.458 | 0.428 | 0.449 |
| $\nu_{LT2}$ (−) | 0.69 | 0.248 | 0.254 | 0.306 |

sampled images. The displacement rate was 0,5 mm per minute. Before measurement, the samples were conditioned at 23 °C and 51% relative humidity. All the tests were performed without delay after the samples had been removed from the conditioning chamber. The measurement recording frequency was 1 Hz. Each frame recorded by the DIC system was compared with the undeformed state in order to calculate the displacement and in-plane strain field e.g Fig. 1(c). The total area of the region used in the image analysis was a centered square of 625 mm2, covering one full face of the cubic sample. This square is corresponding to the facet field of 88 × 90 facets for the DIC measurements. The chosen region of interest is marked by the dashed line in Fig. 1(c) and covers 60% of the cube face. The acquired strain fields were smoothed by averaging of each data pixel with 3 × 3 surrounding pixels in order to avoid undesired spike artifacts in the measured strain field. The strain determined by DIC in the loading direction was plotted against the applied stress, as shown in Fig. 1(d). The choice of strain measure is the subject of a later discussion. The Poisson's ratios $\nu_{xy}$ for all the orthotropic planes were calculated as the negative ratio of the average transverse $\varepsilon_x$ (passive) to the normal $\varepsilon_y$ (compressive and active) strains.

## 3. Results and discussion

The simulated strain results can be used to assess the errors in the estimated elastic parameters and to compare the merits of the different strain measures. There is an unlimited number of parametric simulations that could be made, but we have studied only a set that we consider relevant for wood and composite applications.

### 3.1. Barrelling in isotropic and transversely isotropic material

Young's moduli and Poisson's ratios normalized with respect to the correct values are presented in Fig. 3 as a function of the relative slippage due to platen friction (the slippage factor $\delta/\delta_{max}$) for different values of the initial Poisson's ratio for the (a) isotropic case and (b, c) the transversely isotropic case. The Young's modulus is determined simply as $\overline{\sigma_y}/\varepsilon_y(x, y)$, where $\overline{\sigma_y}$ is the average stress in the whole cube. In all cases, the barrelling leads to an overestimation of the Young's moduli, as shown in Fig. 3(a,b,c), due to the perturbed strain field in the area close to the upper and lower edges, where constrained material has a stiffer response. Noting the difference in scales of the y-axes, it is clear that the error in the

Youngs modulus is much higher for the isotropic than for the transversely isotropic case, and that it is larger in the LT plane (loading in the L direction) than in the TT plane, Fig. 3(b and c). In general, for increasing Poisson's ratio, the error becomes larger. The perturbed zones are shown in Fig. 4 as the local error on the examined face, where the axial strains are visualized in (a), (b), (c) and normalized by division on correct input value. The Poisson's ratio is determined as $-\varepsilon_x(x,y)/\varepsilon_y(x,y)$ and normalized by division on correct input value. In general, for increasing Poisson's ratio, the error becomes larger. For the transversely isotropic material (Fig. 3(b) and (c)) the error in Young's moduli is less in the transverse direction T than in the axial direction L. This difference in behaviour can be discussed by examining the spatial variation of the elastic parameters determined from strain fields for isotropic and transversely isotropic materials. Fig. 4(a−c) shows the patterns of the constraining effect that originate from the top and bottom of the cube face where the sample is in contact with the platens. The constraining effect is significant in the zones within 20% of the height from the horizontal edges of the model. Fig. 3(a') shows that the relative error in the Poisson's ratio is smaller in the isotropic material than in the transversely isotropic materials in Fig. 3(b',c'), and this can also be observed in the corresponding strain ratio field shown in Fig. 4(a', b', c').

The green zones corresponding to a vanishing error are found in the central band of the numerical model. In the transversely isotropic cases, Fig. 4(b') (LT plane) and (c') (TT plane) the error is not-negligible in the central part of the cube face. The effect is stronger in the LT plane, where the perturbed zone extends over a larger area. For instance, for the slippage factor $\delta/\delta_{max} \approx 0.2$ (where $K = 0.1$), the Poisson's ratio is underestimated by 30−40%, cf. Fig. 3(b'). The situation is the same in the TT plane, but the effect is smaller than in the LT plane. In Fig. 4(a'−c'), it can be seen that the constraining effect is significant in the case of the Poisson's ratio. The blue colored area where the error is greater than 5% spreads from the horizontal edges of the model throughout the central region of the material. The most accurate estimation of Poisson's ratio is in the central area close to the vertical edges of the cube as it shown in Fig. 4(b' and c'). However, rosette or crossed strain gauges are usually placed in the centre of the specimen, where the constraint effect persists in transverse isotropic specimens in the LT plane. Full-field DIC measurements allow the direct determination of the Poisson's ratio in the unperturbed zones close to the face edges.
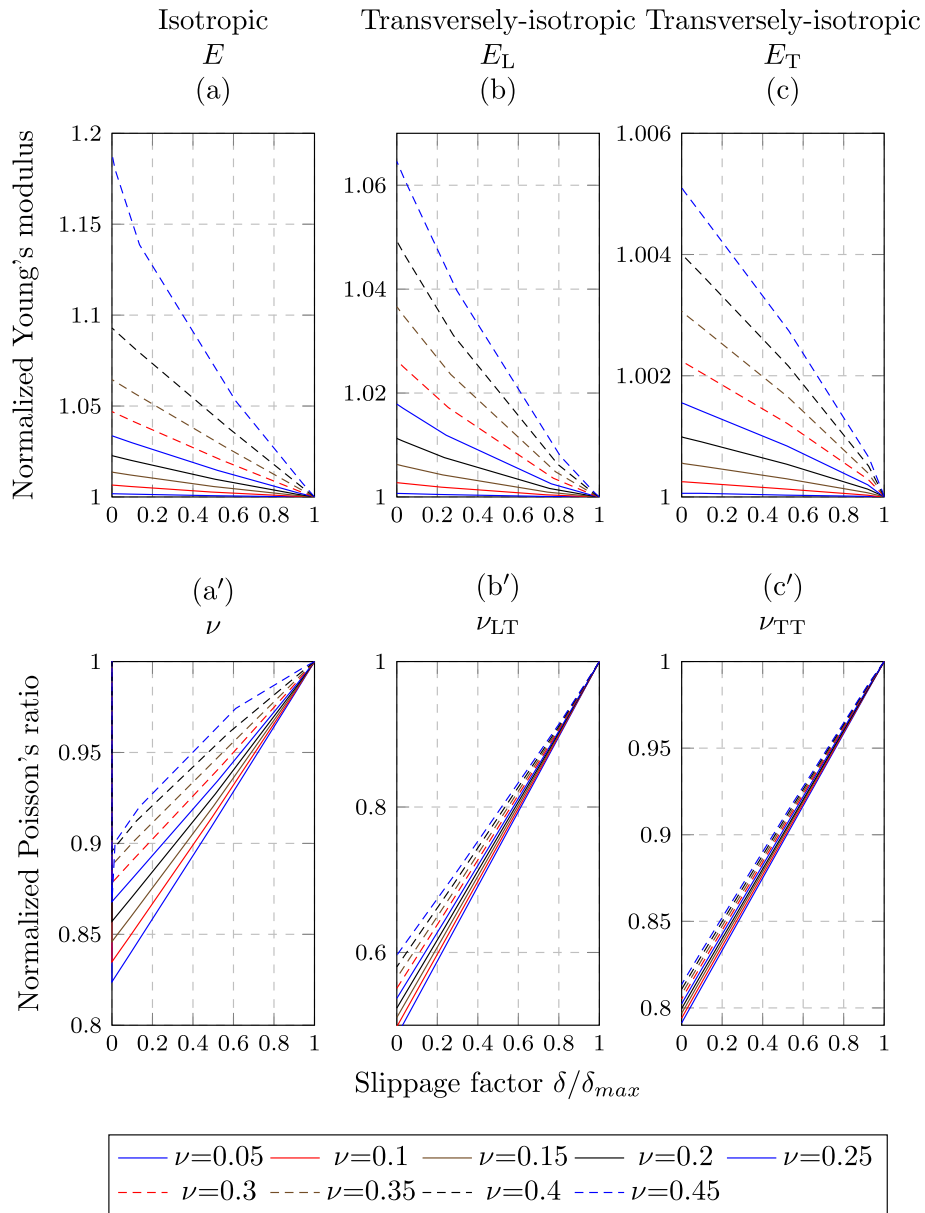
**Fig. 3.** Simulated and normalized Young's moduli and Poisson's ratio of isotropic material ($a = 1$) and transversely isotropic material ($a = 10$; $b = 2$) with initial Poisson's ratio ($\nu$) versus slippage factor. The results were obtained using the full field method.

## 3.2. Effects of strain measurement

The measured Young's moduli and Poisson's ratios vary depending on the strain measurement method employed. In the present work, four methods were used in the simulations and compared. The first method, shown in Fig. 5(a), was a full-field. Here, the error in the Young's moduli originates from the underestimated axial strains that are the reason for the constraining effect close to the platens. The evaluation of Poisson's ratio shows a large error compared to the central band and strain gauge methods due to inclusion of the total surface area in the strain evaluation. In Fig. 4(b), the total area includes the regions close to the constrained regions where the error is dominating.

In the second method, shown in Fig. 5(b), only the middle 60% of the surface area was taken for the determination of strain. The corresponding plot show that this method gives a closest to real value for the Young's moduli comparing to the first method. The

numerical results from the first two methods can be compared with the experimental results in Figure ?? that depicts the strains $\varepsilon_y$ from the Full field (blue) and Central band (red) zones. The numerical result correlates with the experiment, i.e. slope from the Full field zone is larger whereas the one from the Central band zone is lower and more accurate.

In the third method, shown in Fig. 5(c), where the Standard ASTM D143-94 technique with strain gauges was used, the error is very close to that found in second method. This happens because the strain is measured between two points that are in the "Central band" of the sample where the constraining effect is less severe.

Large error values in the Young's modulus close to the horizontal edges of isotropic model are clearly visible in Fig. 4(a). The opposite is true in the case of the transversely isotropic sample in Fig. 4(b and c) in the *LT* plane, the Young's moduli in the central area is overestimated, whereas in the *TT* plane, the strain field is similar to that of the isotropic material.
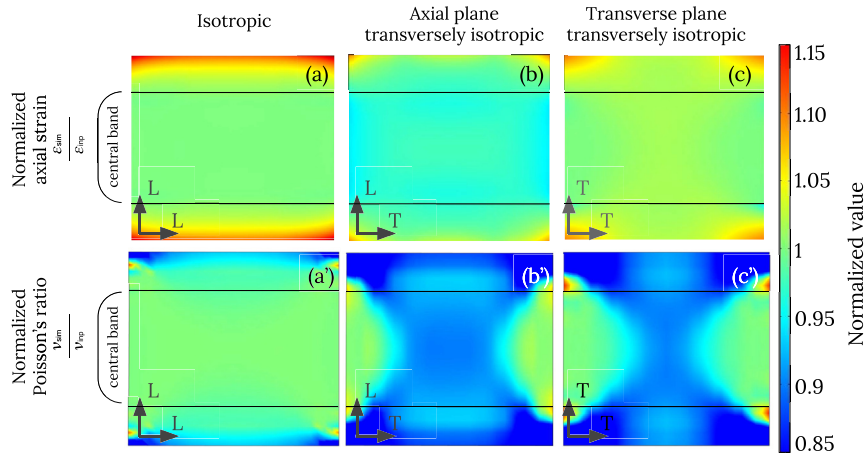
**Fig. 4.** The simulated results for normalized axial strains and Poisson's ratio in different cube sides for isotropic and transversely isotropic materials ($K = 0.1; \nu = 0.3; \delta/\delta_{max} \approx 0.2$).
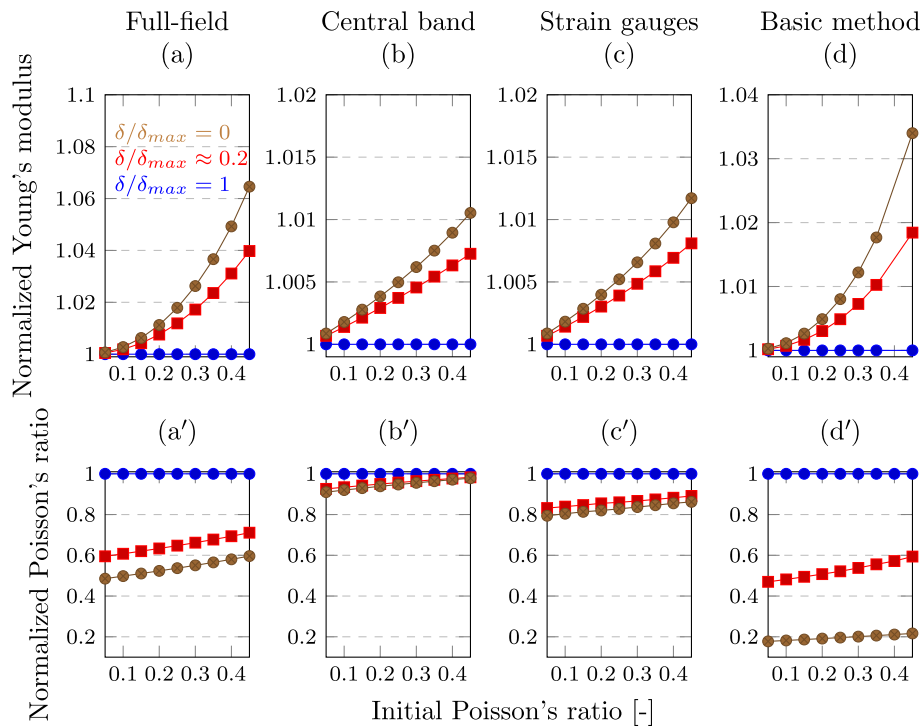


**Fig. 5.** Normalized Young's moduli ($E_L$) and Poisson's ratio ($\nu_{LT}$) vs. the initial Poisson's ratio of transversely isotropic material for different slippage conditions, for to different ways of measuring strain.

These simulations support the simulated results based on experimental data that is presented in Fig. 6, where the average strain diagram for the total area shows a larger Young's moduli than the diagram for the chosen area. Additional outcomes can be deduced from the error fields in Fig. 4(a'–c'). The ASTM-D143-94 standard [22] requires the installation of strain gauges in the centre of the sample, but they leads to an underestimation of Poisson's ratio in a transversely isotropic cubic sample due to the barrelling. On the other hand accurate values are obtained for an isotropic material, where the constraining effect influences the horizontal faces of the sample. The chosen central region of the isotropic sample is most favourable for accurate measurements.

### 3.3. Barrelling in orthotropic material

The barrelling is more severe in an isotropic than in a transversely isotropic material. To check whether this applies to orthotropic materials, a model was simulated based on Vasa material properties that were experimentally determined [5].

The results for the normalized Young's moduli in the orthotropic directions of wood and the Poisson's ratio are plotted in Fig. 6 versus the slippage factor. The notation for the wood planes in Fig. 6 indicates the principal orthotropic directions: Longitudinal (L), Radial (R), Tangential (T).

This figure shows that the magnitude of error for (L) direction is less than for the transversely isotropic material. The Poisson's ratio is underestimated with increasing constraining effect, as was
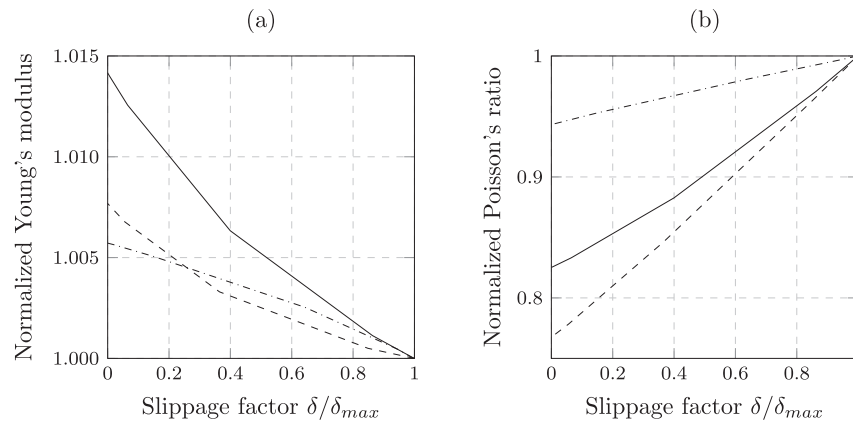
(a)                                                    (b)



**Fig. 6.** Simulated and normalized results based on experiments with an orthotropic material. a) Young's moduli and b) Poisson's ratio, while measuring the strain field from planes LT(−), TL(−), TR(-·-·-).

observed in the orthotropic material simulation. The magnitude of error is less, however. The $\nu_{LT}$, $\nu_{LR}$, $\nu_{TR}$ are less influenced by the barrelling. In contrast, $\nu_{TL}$ is more underestimated than the others, as shown in Fig. 6(b). When the L direction is in the transverse plane, the geometrical response is less significant because of the stiffness of the material. The magnitude of possible error depending on barrelling is therefore larger. However if the $\nu_{LT}$, $\nu_{LR}$, $\nu_{TR}$ ratios are known the symmetry principle [21] can be used to determine the rest.

## 4. Conclusions

This study was initiated due to the problem of obtaining accurate data for the waterlogged PEG-impregnated oak timber of the Vasa ship, and the fact that the material was available in the form of cubic samples. This study has validated the use of cubic samples, and the magnitude of the errors in the elasticity constants arising from the friction between platens and the sample when cubic samples are subjected to compressive tests has been quantified. Taking into account the magnitude of these errors, it will be possible to estimate the right engineering constants of material and to design suitable support for the ship.

Barrelling in cubic samples subjected to compressive testing is a phenomenon that can influence the estimation of the engineering elastic constants. The magnitude of the error depends on the type of material anisotropy, viz. isotropy, transverse isotropy and orthotropy, which are representative of most load-bearing materials:

- *Isotropic* material is affected most by the barrelling. For example, the measured Young's moduli was overestimated by up to 20% for a material with a Poisson's ratio of $\nu = 0.45$. The estimation of Poisson's ratio gives less errors than with other materials.
- *Transversely isotropic* material shows an overestimation of Young's moduli in both the L and T directions but less than the isotropic material. The error is larger for the LT and TT plane in the estimation of the Poisson's ratio.
- *Orthotropic* material was simulated using the experimental input data for the experimentally characterised archaeological wood. The result shows an overestimation of Young's moduli in all principal planes of orthotropic wood, but the error is similar to that in the TT plane in the transversely-isotropic material, which is less than 1.5% error.

The strain measurement methods showed that it was

advantageous to use a 60% of surface area (central band methodology) for the estimation of strains in the corresponding plane. The results can be summarized as follows:

- Using the entire strain field from the *full field* measurement of the sample plane leads to relatively large errors in the estimated elastic properties, since the constrained regions close to the platens form a large part of the strain measurement. In the severe case of rubber-like, almost incompressible materials with $\nu = 0.45$, the measured Young's moduli is overestimated by up to a distressing level of 20%. On the other hand, the estimation of Poisson's ratio gives smaller errors comparable to those in transverse isotropic and orthotropic materials.
- Strains from the *strain gauge* measurement (the standardized method) shows smaller errors in the estimated elastic properties than the full-field method. However, the measurements are made between two points inside the constraining cone emanating from the friction of the platens. Thus, the strain gauge method also leads to non-negligible errors.
- The *central band* of the full-strain field in the centre of the sample was chosen to cover a zone which is relatively unperturbed by the frictional platens in the compressive test. Here, relatively good results with small errors were obtained.

Two strain-field measuring techniques, *full field* and *central band* were used in the experiments. The elastic properties were estimated from the strain measurements in the central band only, as this was shown to be more accurate. Since full-field measurement techniques are becoming more commonplace in mechanical testing laboratories, their advantages over point or line measurements (e.g. strain gauges or extensometers) should be exploited. It is recommended to use the region of the strain field that is only moderately affected by loading constraints from the test rig. In the compressive testing of cubes, a suitable part has been found to be a central lateral band covering 60% of the observed face. As a basis for future work it can be recommended to include the comparison of all experimental methods with the results from the numerical simulations.

## References

[1] G. Tsoumis, et al., Science and Technology of Wood. Structure, Properties, Utilization, Van Nostrand Reinhold, 1991.

[2] ASTM D143-14, Standard Test Methods for Small Clear Specimens of Timber, ASTM International, West Conshohocken, PA, 2014, http://dx.doi.org/10.1520/d0143.

[3] S. Johnson, L. Daniel, S. Avva, A. Chamis, R. Reddy, W. Haag, R. Chait, C. Yao, E. Guess, N. Lamothe, et al., Compression testing of homogeneous materials and composites, in: Compression Testing of Homogeneous Materials and Composites, ASTM International, 1983.

[4] J. Ljungdahl, L.A. Berglund, Transverse mechanical behaviour and moisture absorption of waterlogged archaeological wood from the vasa ship, Holzforschung 61 (3) (2007) 279–284.

[5] A. Vorobyev, O. Arnould, D. Laux, R. Longo, N.P. van Dijk, E.K. Gamstedt, Characterisation of cubic oak specimens from the vasa ship and recent wood by means of quasi-static loading and resonance ultrasound spectroscopy (rus), Holzforschung, doi:10.1515/hf-2015-0073.

[6] H. Toftegaard, Simulated stiffness determination from simple compression tests on a thick laminate, Compos. A 30 (7) (1999) 849–858, http://dx.doi.org/10.1016/S1359-835X(98)00199-7.

[7] P. Oldroyd, P. Benham, Stress-strain behaviour of copper and zinc cubes subjected to cyclical compression, Int. J. Mech. Sci. 8 (2) (1966) 77–88.

[8] A. Majano-Majano, J. Fernandez-Cabo, S. Hoheisel, M. Klein, A test method for characterizing clear wood using a single specimen, Exp. Mech. 52 (8) (2012) 1079–1096.

[9] F. Pierron, M. Grédiac, The Virtual Fields Method: Extracting Constitutive Mechanical Parameters from Full-field Deformation Measurements, Springer Science & Business Media, 2012.

[10] F. Gillard, R. Boardman, M. Mavrogordato, D. Hollis, I. Sinclair, F. Pierron, M. Browne, The application of digital volume correlation (dvc) to study the microstructural behaviour of trabecular bone during compression, J. Mech. Behav. Biomed. Mater. 29 (2014) 480–499.

[11] Y. Huang, L. Liu, F. Sham, Y. Chan, S. Ng, Optical strain gauge vs. traditional strain gauges for concrete elasticity modulus determination, Optik-Int. J. Light Electron Opt. 121 (18) (2010) 1635–1641.

[12] J. Xavier, A. De Jesus, J. Morais, J. Pinto, Stereovision measurements on evaluating the modulus of elasticity of wood by compression tests parallel to the grain, Constr. Build. Mater. 26 (1) (2012) 207–215.

[13] A. Odgaard, F. Linde, The underestimation of young's modulus in compressive testing of cancellous bone specimens, J. Biomech. 24 (8) (1991) 691–698.

[14] K. Dahl, K. Malo, Planar strain measurements on wood specimens, Exp. Mech. 49 (4) (2009) 575–586.

[15] T. Ozyhar, S. Hering, P. Niemz, Moisture-dependent orthotropic tension-compression asymmetry of wood, Holzforschung 67 (4) (2013) 395–404.

[16] I. Bjurhager, H. Halonen, E.-L. Lindfors, T. Iversen, G. Almkvist, E.K. Gamstedt, L.A. Berglund, State of degradation in archeological oak from the 17th century vasa ship: substantial strength loss correlates with reduction in (holo) cellulose molecular weight, Biomacromolecules 13 (8) (2012) 2521–2527.

[17] T.-K. Chen, Compression Test Simulation of Thick-section Composite Materials, in: Tech. Rep., 1992. DTIC Document.

[18] Comsol Multiphysics Version 4.4. User's Guide, COMSOL, 2014.

[19] R. Narayanasamy, R. Murthy, K. Viswanatham, G. Chary, Prediction of the barreling of solid cylinders under uniaxial compressive load, J. Mech. Work. Technol. 16 (1) (1988) 21–30, http://dx.doi.org/10.1016/0378-3804(88)90136-2.

[20] K. Kulkarni, S. Kalpakjian, A study of barreling as an example of free deformation in plastic working, J. Eng. Ind. 91 (3) (1969) 743–754.

[21] M.W. Hyer, Stress Analysis of Fiber-reinforced Composite Materials, DEStech Publications, Inc, 2009.

[22] ASTM E9–89a(2000), Standard Test Methods of Compression Testing of Metallic Materials at Room Temperature, ASTM International, West Conshohocken, PA, 2009, http://dx.doi.org/10.1520/e0009-89ar00.